JACS
JOURNAL OF THE AMERICAN CHEMICAL SOCIETY
pubs.acs.org/JACS
Article

Anchorage-Dependent Living Supramolecular Self-Assembly of Polymeric Micelles

Zhengmin Tang,[†] Liang Gao,[†] Jiaping Lin,* Chunhua Cai,* Yuan Yao, Gerald Guerin,* Xiaohui Tian, and Shaoliang Lin

Cite This: *J. Am. Chem. Soc.* 2021, 143, 14684−14693

ABSTRACT: Anchorage-dependent contact-inhibited growth usually refers to on-surface cell proliferation inhibited by the proximity of other cells. This phenomenon, prominent in nature, has yet to be achieved with polymeric micelles. Here, we report the control living supra-macromolecular self-assembly of elongated micelles with a liquid crystalline core onto a hydrophobic substrate via the synergetic interactions between the substrate and aggregates dispersed in solution. In this system, seed formation is a transient phenomenon induced by the adsorption and rearrangement of the core-swollen aggregates. The seeds then trigger the growth of elongated micelles onto the substrate in a living controllable manner until the contact with the substrate is disrupted. Brownian dynamic simulations show that this unique behavior is due to the fusion of the aggregates onto both ends of the anchored seeds. More important, the micelle length can be tuned by varying the substrate hydrophobicity, a key step toward the fabrication of intricate structures.

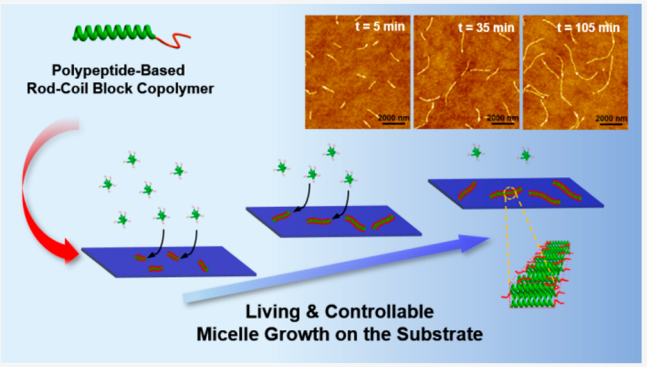

INTRODUCTION

A large category of cells like neurons, muscle cells, and fibroblasts are anchorage dependent and can only survive when deposited onto a substrate,[1] where they thrive, dividing and growing. Such cells are contact-inhibited, and the presence of defects[2] or other cells[3] leads to growth disruption. The development of nanostructures that would share, even partially, some common features with these fundamental biological systems is a daunting task that requires multiple complex steps and involves various scientific fields. Among those, polymer science, via block copolymer (BCP) self-assembly in solution, has already shown excellent abilities to mimic biological objects like vesicles[4,5] and amyloid fibrils.[6,7]

To obtain a truly anchorage-dependent contact-inhibited micelle growth, the micelle core should strongly interact with the substrate. At first sight, such specification seems prohibitive since micelle growth requires the core-forming block to be mobile enough to add onto the extremities of the growing micelles. In the recent examples that have been reported of elongated micelles grown onto surfaces by crystallization-driven self-assembly[8−10] (CDSA), the corona-forming block is used as a linkage that keeps the micelles attached to the surface. Such a system, however, is not anchorage-dependent, and the micelles can still grow when the corona does not touch the substrate, allowing micelles to protrude into the solution[8] or to cross each other on the substrate, which leads to undesired networking.[10]

As a first step toward the fabrication of anchorage-dependent cell-like nanostructures, we focus, here, on the preparation of 1D micelles that would grow in a living manner only via intimate contact with the substrate. To reach the delicate balance between micelle adhesion and growth, we foresaw that the core of the micelle should firmly adhere to the substrate while being mobile enough to rearrange onto the surface as it grows. Owing to liquid crystals' unique ability, which combines fluidity and order and allows them to anchor and align onto specific surfaces,[11−15] we expected polymeric micelles with a liquid-crystalline core to be appropriate candidates.

We thus studied the self-assembly of a rod−coil BCP that forms micelles with a liquid−crystalline core in a solvent mixture selective for the coil block. In the absence of a substrate, small aggregates were formed and remained stable in solution; however, the presence of a hydrophobic substrate

Received: June 10, 2021
Published: September 2, 2021

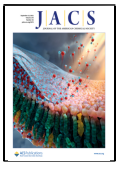

https://doi.org/10.1021/jacs.1c06020
J. Am. Chem. Soc. 2021, 143, 14684−14693

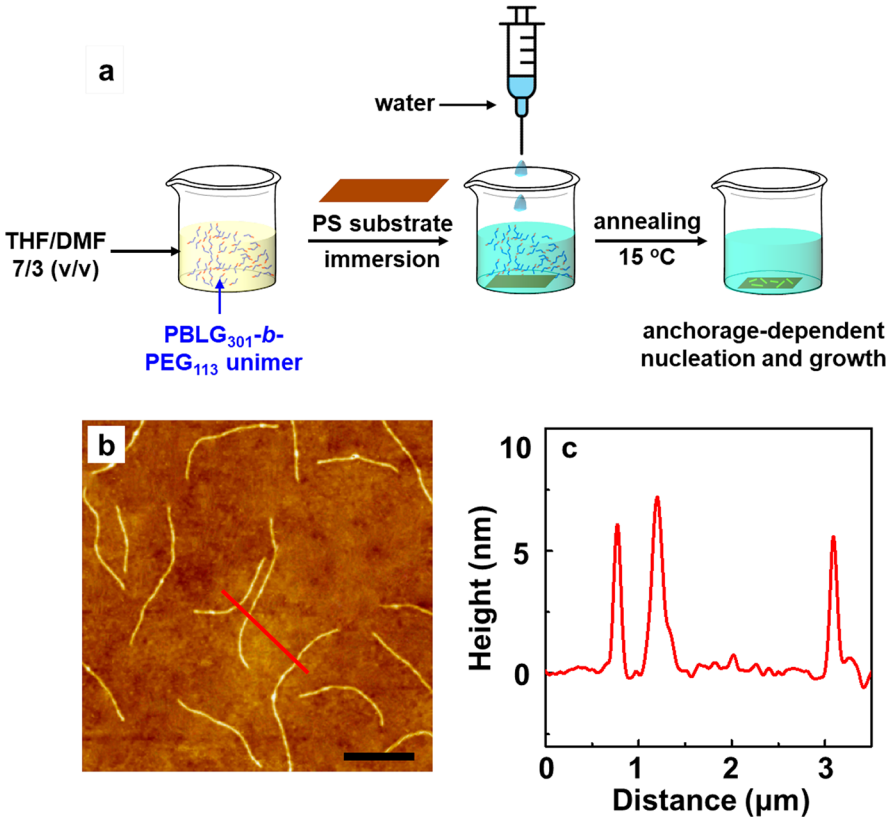

Figure 1. Anchorage-dependent growth procedure. (a) Sample preparation: a unimer solution of $PBLG_{301}$-*b*-PEG_{113} (c = 0.05 mg mL^{-1}) was prepared in a mixture of THF/DMF: 7/3 (v/v). A PS-coated silicon substrate was then immersed before water was added dropwise to reach 13.3 vol %. After 2 h of aging, the substrate was taken out of the solution and observed by AFM (b). (c) Height profile of the micelles. The scale bar in the AFM image is 2000 nm.

during the formation of the small aggregates induced their adsorption and triggered the growth of 1D micelles anchored to the substrate.

We found that the micelle length can be tuned, with a relatively narrow length distribution, and more important, that they can be further elongated when reimmersed in another BCP solution, features that are found in controlled living systems such as controlled/living polymerization[16] and CDSA.[17−19] This anchorage-dependent growth was confirmed by Brownian dynamics (BD) simulations that show how the substrate promotes the reorganization of the micelle core and favors the formation of 1D micelles via synergetic interactions between the substrate, the seeds, and the small aggregates in solution. Finally, we demonstrated the crucial role of the micelle core/substrate interactions by preparing micelles of different lengths at different degrees of substrate hydrophobicity.

RESULTS AND DISCUSSION

Anchorage-Dependent Living Growth of Cylindrical Micelles. Poly(γ-benzyl-L-glutamate) (PBLG) is a hydrophobic rodlike polypeptide with an α-helical rigid conformation. When copolymerized with a hydrophilic block such as poly(ethylene glycol) (PEG), the resulting rod−coil block copolymer (BCP) undergoes micellization in selective solvents for the hydrophilic block, forming structures with a liquid crystalline core.[20−24] In the present study, we first prepared a unimer solution of $PBLG_{301}$-*b*-PEG_{113} (the subscripts refer to the degree of polymerization of the corresponding block) by dissolving the BCP in a mixture of THF/DMF = 7/3 (v/v) (where THF stands for tetrahydrofuran and DMF for *N*,*N*-dimethylformamide) at a concentration, c, equal to 0.05 mg mL^{-1}. Small aggregates with a PBLG core and a PEG corona were then obtained by the dropwise addition of water to 13.3 vol %, above the critical water content (CWC) of ca. 10.7 vol % (Figure S1). The small aggregates were uniform in size with a mean diameter of ca. 100 nm as measured by atomic force microscopy (AFM, Figure S2a) and transmission electron microscopy (TEM, Figure S2b). These micellar aggregates were stable in solution (Figure S3).

Interestingly, when water was added dropwise above 10.7 vol % of a THF/DMF (7/3, v/v) solvent mixture containing $PBLG_{301}$-*b*-PEG_{113} unimer (c = 0.05 mg mL^{-1}) in the presence of a polystyrene (PS) film irreversibly coated on a silicon wafer (Figure 1a and Figure S4), the behavior of the system changed drastically. After the substrate was incubated for 2 h, we could observe the presence of discrete elongated micelles on the substrate by AFM (Figure 1b). These micelles were ca. 90 nm wide with a height of approximately 7 nm (Figure 1c) and a number-average length, L_n, of 3460 ± 809 nm. The width of the micelles deposited on the substrate appears to be directly related to the length of the PBLG block. For example, the self-assembly of $PBLG_{164}$-*b*-PEG_{113} and $PBLG_{320}$-*b*-PEG_{226} BCPs in the presence of a PS-coated silicon substrate led to the formation of 58 nm ($PBLG_{164}$-*b*-PEG_{113}) and 105 nm ($PBLG_{320}$-*b*-PEG_{226}) wide micelles, respectively (Figure S5). In addition, the large majority of the micelles observed by AFM possessed a ca. 13 nm high brighter dot that corresponds to a thicker section of the micelles (Figure 1b). These sections

https://doi.org/10.1021/jacs.1c06020
J. Am. Chem. Soc. 2021, 143, 14684−14693

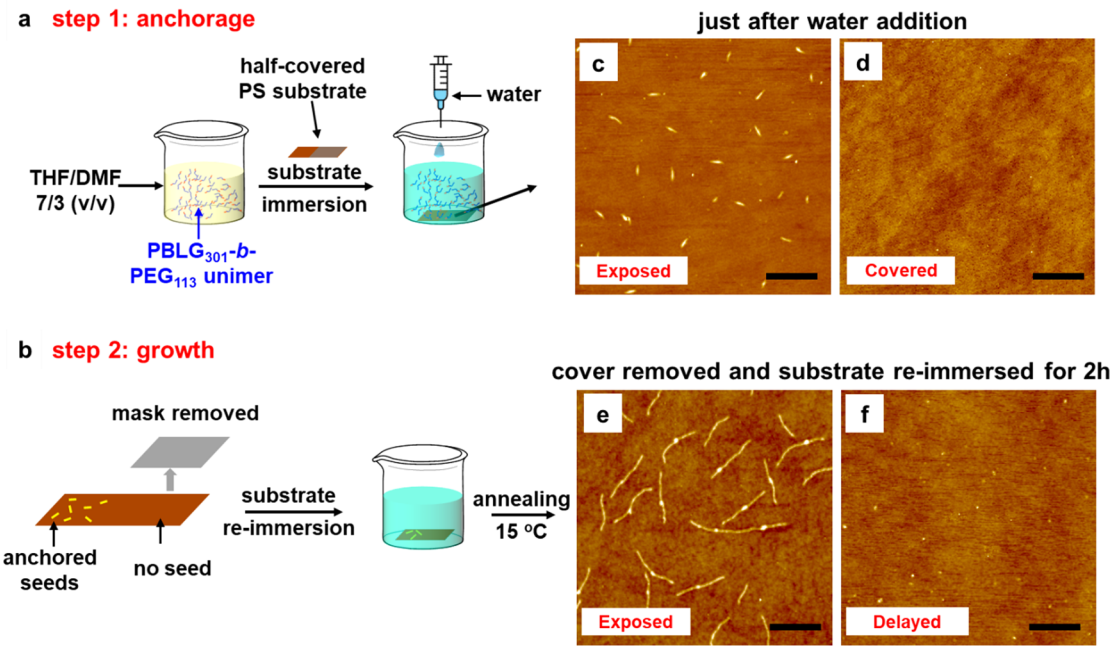

Figure 2. Delayed exposure of the PS-coated silicon substrate. The experiment was performed in two steps. Step 1 (a): a unimer solution of $PBLG_{301}$-*b*-PEG_{113} (c = 0.05 mg mL^{-1}) was prepared in a mixture of THF/DMF 7/3 (v/v). A PS-coated silicon substrate partly covered in a lap-shear joint geometry (Figure S6) was then immersed, and water was added dropwise to reach 13.3 vol %. Step 2 (b): the mask was removed after the substrate was taken out from the solution, and the substrate was rinsed and reimmersed in the same solution for 2 h. (c,d) AFM images of the exposed (c) and covered (d) sections of the substrate after step 1. (e,f) AFM images of the exposed (e) and uncovered (f) sections of the substrate after step 2. The scale bars in the AFM images are 2000 nm.

might be either the starting seeds of the micelles or structural defects occurring during micelle growth.

To confirm the crucial role of the PS-coated silicon substrate, we performed a two-step experiment to delay the exposure of one-half of the substrate to the solution until after water addition (Figure 2a,b). As expected, relatively short (ca. 500 nm) elongated micelles were present on the exposed part of the PS-coated silicon substrate (Figure 2c,d) after water addition. Surprisingly, however, when we looked at the substrate reimmersed for 2 h (Figure 2e,f), we could observe elongated micelles on the initially exposed section of the substrate, while the second half only showed small aggregates that seemed to have deposited onto the substrate during incubation. The absence of elongated micelles on the second half of the PS-coated silicon substrate at the end of step 2 indicates that the nucleation window is extremely narrow and only occurs during water addition. Indeed, the minute spent to remove the mask, rinse, and reimmerse the sample into the solution was already too long for secondary nucleation to occur. Even more striking was the increase in length of the micelles deposited onto the PS-coated silicon substrate, which grew from ca. 500 nm prior reimmersion to ca. 2.2 μm after 2 h of incubation (Figure S7).

Living Growth of the Cylindrical Micelles. The ability of the seeds to extend once the substrate was reimmersed into a micelle solution represents a key aspect of living growth. This observation alone, however, is not sufficient to claim excellent control over micelle length. Other features are also particularly important to confirm that the anchorage-dependent growth presented here is indeed living and controllable:[25,26] the micelles should extend in the presence of additional polymer and their lengths should increase linearly as a function of the amount of polymer present in solution.

The most convincing proof that the anchorage-dependent growth was living came from an iterative incubation experiment (Figure 3 and Figures S8–S10). We first prepared relatively short seeds with a narrow length distribution via the surface-mediated protocol depicted in Figure 1a (L_n = 850 ± 155 nm, Figure 3a,e), incubating the PS-coated silicon substrate for only 5 min. We then took the PS-coated silicon substrate out of the solution and rinsed it with a THF/DMF/water mixture (THF/DMF = 7/3 v/v, water content = 13.3 vol %), we immersed it in another micelle solution (THF/DMF = 7/3 v/v, c = 0.02 mg mL^{-1}, water content = 13.3 vol %), prepared in the absence of substrate. After 10 min of incubation time, the seed lengths increased from $L_n \approx 850$ to $L_n \approx 1200$ nm, confirming undeniably that the micelle seeds attached to the substrate were still active and could grow in a living manner. During this first incubation period, the number-average micelle lengths, L_n, first increased rapidly as a function of incubation time (Figure 3i) before reaching a plateau at $L_n \approx 1800$ nm (Figure 3b,f) when the incubation time was larger than 100 min.

The presence of a plateau suggested that most of the polymer chains were consumed by the micelle growth. We took the substrate out of the solution, rinsed it, and reimmersed it into a newly prepared micelle solution (THF/DMF = 7/3 v/v, c = 0.02 mg mL^{-1}, water content = 13.3 vol %) for a second incubation period. This subsequent growth step led to micelle elongation following the exact same pattern: The micelles grew very rapidly at short times before reaching a plateau at $L_n \approx 2500$ nm (Figure 3c,g). A third incubation period finally further confirmed the high reproducibility of our procedure (Figure 3d,h).

The livingness of the anchorage-dependent growth reported here can be further emphasized in Figure 3j. In this plot, we

https://doi.org/10.1021/jacs.1c06020
J. Am. Chem. Soc. 2021, 143, 14684–14693

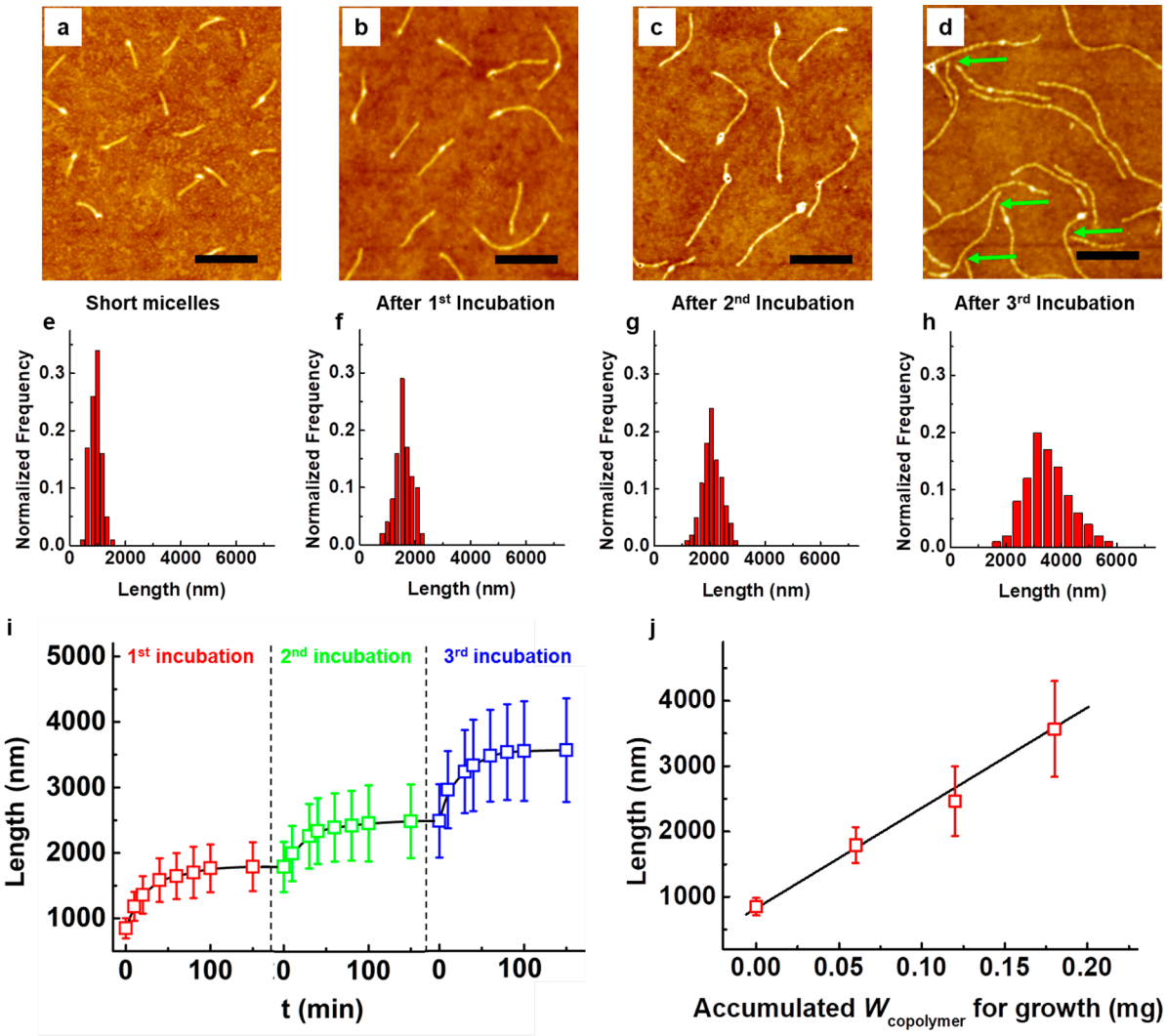

Figure 3. Iterative incubation experiment. A unimer solution of $PBLG_{301}$-*b*-PEG_{113} (c = 0.02 mg mL^{-1}) was prepared in a mixture of THF/DMF: 7/3 (v/v). A PS-coated silicon substrate was then immersed before water was added dropwise to reach an amount of 13.3%. After 5 min of aging, the substrate was taken out of the solution and observed by AFM (a) to evaluate their length distribution (e). The substrate was then immersed in newly prepared aggregate solutions for three successive incubation periods of 2 h each. (b–d) AFM images and corresponding length distributions (f–h) of the micelles at the end of each incubation step. (i) Plot of the micelle length as a function of time for the three incubation periods. (j) Plot of the number-average length of the micelles at the end of each incubation period as a function of the accumulated weights of copolymers ($W_{copolymer}$) used for micelle growth. The scale bars in the AFM images are 2000 nm.

show that the number-average length of the micelles at the end of each incubation period (once the plateau was reached) increased linearly as a function of the cumulative amount of polymer used. In addition, the contour length histograms of the elongated micelles only contained one micelle population, confirming that there was no secondary nucleation after incubation (Figure 3e–h). This is a crucial and remarkable result, emphasizing the unique features of anchorage-dependent growth.

Because the anchorage-dependent growth demonstrated striking similarities with living polymerization, one would also expect the length distributions of the micelles to be narrow throughout the three incubation periods. This was, however, not the case, especially for the third incubation period (Figure 3d,h). Paradoxically, the broadening of the micelle length distribution finds its origin in the intrinsic nature of micelle anchorage-dependent contact-inhibited growth. By definition, the anchorage-dependent growth of a given micelle should end when its adhesion to the substrate is disrupted, leading to a contact-inhibited growth. This is the case when one micelle crosses the path of a second micelle, as pointed out by green arrows in Figure 3d, an event that becomes more frequent as the micelles grow longer. Over the thousands of micelles imaged, we could not find any cases where two micelles crossed each other.

While we ascertained that the anchorage-dependent growth was a living process, we still needed to clarify the exact nature of the units that grow onto the seeds. Since we observed that small aggregates formed in solution (Figure S2) when water was added to a THF/DMF polymer solution, we hypothesized that they were involved in the seeded growth. Two main pathways were considered. (i) The micelles suspended in solution could serve as reservoirs by releasing unimer that would, later on, add onto the seeds, or (ii) they would directly merge with the seeds, elongating them.

To test if the seed growth was the result of the addition of unimer onto their both ends, we deposited $PBLG_{301}$-*b*-PEG_{113} seeds (L_n = 530 ± 120 nm, Figure 4a,c) onto a PS-coated

https://doi.org/10.1021/jacs.1c06020
J. Am. Chem. Soc. 2021, 143, 14684–14693

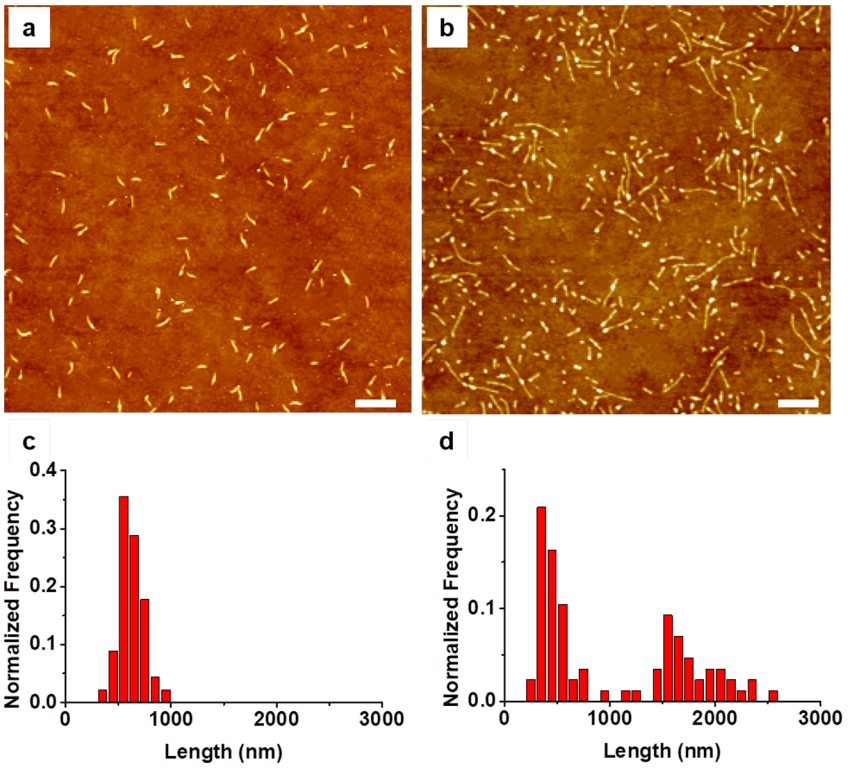

Figure 4. Effect of unimer addition. (a) AFM image of a PS-coated silicon substrate covered with seeds obtained after 5 min incubation. The substrate was immersed in a mixture of THF/DMF/water (THF/DMF = 7/3 v/v, water content = 13.3 vol %). In a second step, a 50 μL unimer solution of $PBLG_{301}$-*b*-PEG_{113} in a mixture of THF/DMF 7/3 (v/v) (c = 1 mg mL^{-1}) was injected into the solution. After 2 h of incubation time, the substrate was taken out of the solution and observed by AFM (b). The corresponding length distributions of the seeds are shown in (c) for the starting seeds and (d) for the sample incubated for 2 h. The scale bars in the AFM images are 2000 nm.

silicon substrate following the surface-mediated protocol depicted in Figure 1a. We then immersed the substrate in a THF/DMF/water mixture (THF/DMF = 7/3 v/v, water content = 13.3 vol %) and injected 50 μL of a solution of $PBLG_{301}$-*b*-PEG_{113} dissolved into a mixture of THF/DMF: 7/3 (v/v) (c = 1 mg/mL) (Figure 4). The amount of unimer added was chosen to match the amount of polymer used for the first incubation experiment (Figure 3). While after 2 h of incubation, the seeds had grown longer, there were striking differences with the previous experiments (Figures 2 and 3). The extended seeds were short, their length distribution was broad with two distinct populations (Figure 4b,d), and interestingly, the number of seeds adsorbed on the substrate after incubation (ca. 0.65 seeds/μm^2) was significantly larger than before unimer addition (ca. 0.34 seeds/μm^2), a clear indication that secondary nucleation occurred.

The obvious lack of control over seed extension when compared to our previous results (Figures 2 and 3) suggests that seed growth via unimer addition is an unlikely pathway. Indeed, if pathway (i) was favored and unimer were adding onto the seeds, one would expect the seeds to grow uniformly, similarly to what we observed in the iterative incubation experiment (Figure 3). Instead, we suspect that the unimer aggregated shortly after they added to the solution. Some of the swollen aggregates then anchored on the substrate (secondary nucleation), while other aggregates added onto the seeds already present on the substrate, leading to the formation of two distinct populations. The increase in the number of seeds via secondary nucleation, thus, led to a decrease in the number-average length of the micelles after 2 h incubation ($L_n \approx 960$ nm) compared to that of the micelles grown after the first incubation period ($L_n \approx 1800$ nm, Figure 3b,f).

Theoretical Simulation and Mechanism. We clarified the role of the small aggregates suspended in solution on the anchorage-dependent growth (pathway (ii)) by performing Brownian dynamics (BD) simulations (see the Methods and Supporting Information).[27] Our purpose here was to investigate the change in the internal structure of the small aggregates once they were deposited onto the substrate and to evaluate how these internal changes could impact micelle growth. Our simulation (Figure 5) first confirms that the anchorage-dependent growth is a supramolecular process that involves the fusion of an aggregate dispersed in solution with a seed anchored on the substrate. It also shows a noticeable morphological differences between the small aggregates suspended in solution and the seeds deposited on the substrate. We evaluated the change in the orientation of the PBLG rod blocks perpendicular to the aggregate long axis (Figure 5b) before and after deposition on a hydrophobic substrate. This orientation is described by the tilt angles ϕ and ϕ' (Figure 5b) and their corresponding standard deviations.[28] We plotted the distribution of cos (ϕ) and cos (ϕ') of the PBLG located inside a deposited seed (green circles) and those inside an aggregate in suspension (blue circles). As shown in Figure 5b, the values of cos (ϕ) and cos (ϕ') are narrowly distributed around 0 for the rod blocks in the seed, while the distribution in the cosine values for those in the aggregate is much broader. The PBLG rod blocks of the micelles deposited on the PS-coated silicon substrate appear to align side-by-side in an interdigitated manner resembling a liquid crystalline structure, in a plane parallel to that of the PS-coated silicon

https://doi.org/10.1021/jacs.1c06020
J. Am. Chem. Soc. 2021, 143, 14684−14693

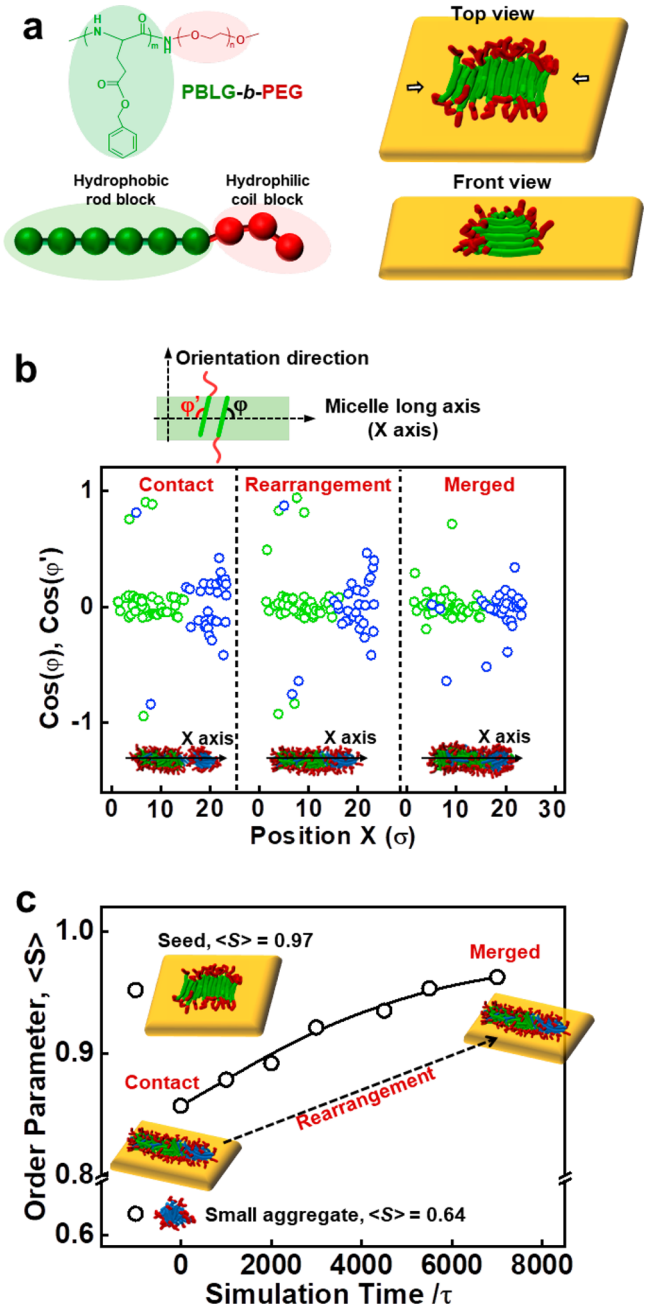

Figure 5. Chain rearrangements revealed by simulations during micelle growth. (a) BD model of rod−coil BCP. Top view and front view of cylindrical micelles deposited on the substrate, showing the partially exposed ends of the micelles. The black arrows mark the micelle ends. (b) Definition of the tilt angles ϕ and ϕ' of the rod blocks. The bottom graph reveals the variation of the values of cos (ϕ) and cos (ϕ') during chain rearrangement for the rod blocks located in the seeds (green circles) and those located in a merging micelle (blue circles). For clarity, the rod blocks in the seeds are colored in green, while those located inside the aggregates suspended in solution are colored in blue. (c) Order parameter ($\langle S \rangle$) of the rod blocks in the elongating micelles during seeded growth.

substrate. In addition, we could observe that the coil blocks (shown in red in Figure 5) could not fully cover both the top and the ends of the seeds. Simulation of an aggregate entering into contact with a seed shows that the alignment of the rod blocks propagates along the aggregate as it merges with the seed, leading to a narrowing of the distribution of the values of cos (ϕ) and cos (ϕ') around 0 (Figure 5b).

The rearrangement of the rod block inside an aggregate as it merges with a seed can be confirmed when one looks at the evolution of the order parameter $\langle S \rangle$ of the rod blocks within the seeds (Figure 5c). As one would expect for a well-aligned structure, the value of $\langle S \rangle$ for a seed before adding a new aggregate is close to 1.0. In comparison, the order parameter of an aggregate in solution is much lower than 1 ($\langle S \rangle = 0.64$). As the aggregate merges with the seed, it induces a decrease in the value of $\langle S \rangle$ for the seed-aggregate structure. $\langle S \rangle$ then increases back to 1 as the alignment of the block in the original seed propagates into the newly added section, allowing the subsequent addition of small aggregates and extending the micelles on the substrate.

The morphological transformation of the micelles as they merge with the seeds represents a key finding of our simulations. This result highlights the role of the core mobility on the anchorage-dependent growth, as well as the synergetic interactions between the seeds and the PS-coated silicon substrate, allowing us to rationalize how seed nucleation occurs. We found that the slow addition of water leads first to the formation of small aggregates with a swollen PBLG core surrounded by a PEG corona. At this early stage of micelle formation, the PBLG rod blocks are mobile inside the micelle core, and the corona does not completely cover it. When such a swollen micelle enters into contact with the substrate, the PBLG liquid−crystalline core anchors to it, most likely via hydrophobic interactions between PBLG and PS, and rearranges quasi instantaneously to form a seed. The swollen stage of the micelles, however, is transient.[29] Adsorption of the PBLG-*b*-PEG aggregates can thus only occur during a very narrow time window. Indeed, as the PBLG core deswells,[30] it decreases its surface area and favors a better coverage by the PEG corona. The corona would then limit the interactions between the PBLG core and the PS-coated silicon substrate, preventing additional seed formation. This latter effect is, however, counterbalanced when seeds are already present on the substrate. Interactions between those seeds and the small aggregates in solution help increase the contact time between the micelles and the substrate, facilitating their attachment and resulting in anchorage-dependent growth (Figure 5b,c) by promoting the reorientation of the PBLG rod block in the micelle core.

The role of the anchorage strength of the PBLG liquid-crystalline core on the anchorage-dependent growth of the micelles was further understood by building a phase diagram (Figure S11) presenting the change in morphology of the structures formed as a function of the rod−rod and rod−polystyrene interaction parameters. Weak interactions limit seed nucleation and growth, hampering micelle anchorage onto the surface. In extreme cases, when the interactions are negligible, the anchorage of seeds onto the substrate would be suppressed.

To evaluate how the micelle/substrate interactions could affect the anchorage-dependent supra-macromolecular self-assembly of $PBLG_{301}$-*b*-PEG_{113}, we performed growth experiments on two different substrates: poly(methyl methacrylate) (PMMA) which is less hydrophobic than PS, and poly(2-vinylpyridine) (P2VP) which is more hydrophilic. When PMMA was used, only a few short cylindrical micelles could be observed (Figure 6a), while for the hydrophilic P2VP substrate, no aggregates were formed (Figure 6b). Encouraged

https://doi.org/10.1021/jacs.1c06020
J. Am. Chem. Soc. 2021, 143, 14684−14693

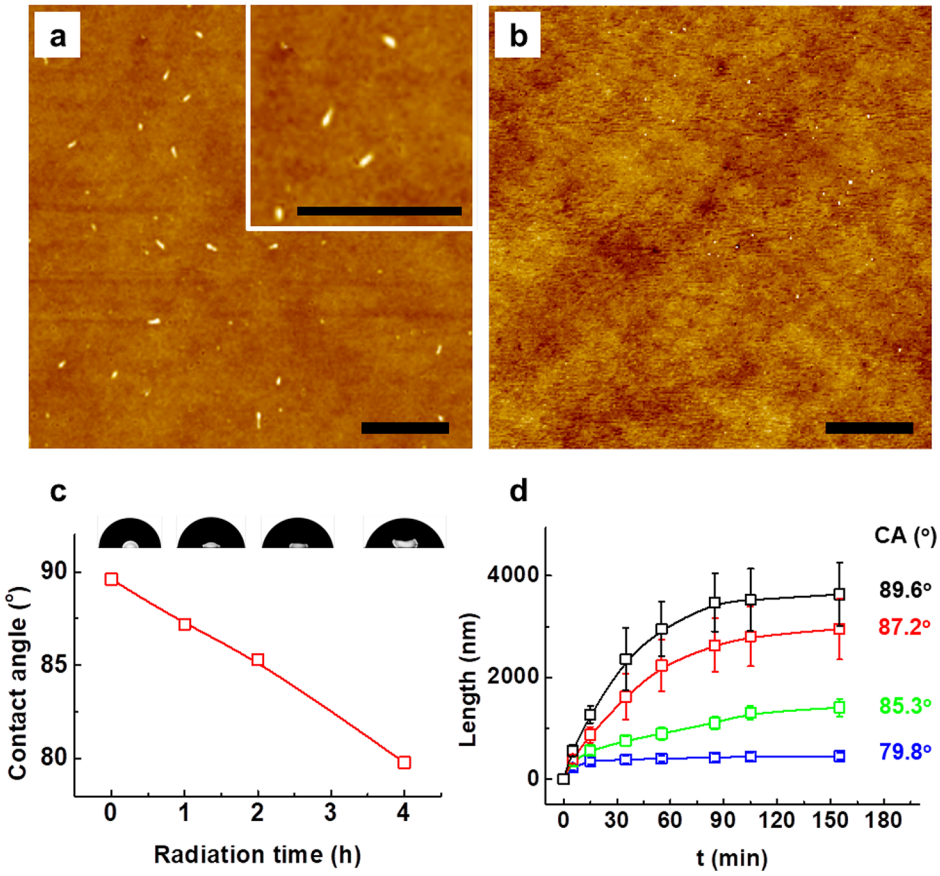

Figure 6. Effects of substrate hydrophobicity on the anchorage-dependent growth. (a,b) AFM images of the structures self-assembled from $PBLG_{301}$-*b*-PEG_{113} on the substrates of (a) PMMA and (b) P2VP. The samples were incubated in solution for 2 h. The samples were prepared according to the protocol shown in Figure 1a. (c) Profile of the water contact angle (with the corresponding value) of the PS-coated silicon substrate after various UV radiation times. (d) plot of L_n versus incubation time for PS-coated silicon substrates with contact angles shown in (c). The scale bars in the AFM images are 2000 nm.

by these results, we decided to investigate the impact of more subtle changes in substrate hydrophobicity. We thus tuned the hydrophobicity of a PS-coated silicon substrate by introducing oxygen-containing groups onto the substrate via UV radiation (Figure 6c,d and Figures S12−S15).[31] After 4 h of UV irradiation, the contact angle of a water droplet on the PS-coated silicon substrate decreased from 89.6° to 79.8°, a clear indication that the surface hydrophilicity increased. As can be seen in Figure 6d, lower surface hydrophobicity (weaker interactions between the substrate and the micelles) led to the formation of shorter micelles. This was especially noticeable when the contact angle reached 79.8°, since no obvious micelle growth could be observed as a function of incubation time (Figure 6d). Those observations are particularly appealing in the context of fabricating intricate structures that would be dictated by local anchoring strengths.[32]

CONCLUSION

Biomimicry has long been an efficient way to prepare sophisticated structures with enhanced properties. In polymer science, vesicles[4,5] and amyloid fibrils[6,7] have been mimicked by polymersomes and 1-dimensional (1D) core-crystalline micelles via the solution self-assembly of BCPs. Since they were first reported, these micelles have evolved from being "simple" mimics toward sophisticated nano-objects[33] that are promising tools for biomedical[34−38] and electronic[10,39,40] applications. Here, the living and controllable anchorage-dependent growth of elongated micelles composed of polypeptide-based BCPs can be seen as a first step toward the fabrication of anchorage-dependent structures.

The supramolecular anchorage-dependent process takes advantage of some key characteristics of liquid crystals and polymer self-assembly. Seeds deposit on the substrate during the transient step of micelle formation and core deswelling, leading to a narrow nucleation time window and to the preparation of micelles of tunable length. In addition, the liquid crystalline core of the aggregates can rearrange once they anchor and merge with the seeds onto the substrate, further elongating the micelles. BD simulations confirmed that the interactions between the substrate and the seeds enhanced the packing of the PBLG blocks, which triggers micelle growth on the substrate. We also showed that the nature of the substrate can strongly affect micelle growth, opening the door to the formation of intricate structures by varying the substrate properties.

EXPERIMENTAL SECTION

Materials. Polystyrene (PS, M_n = 537 kDa, $Đ$ = 1.03) was purchased from Polymer Standards Service. Toluene (HPLC grade) and *α*-methoxy-*ω*-amino poly(ethylene glycol) (mPEG-NH_2, M_n = 5 kDa and 10 kDa) were purchased from Sigma-Aldrich. *γ*-Benzyl-L-glutamate-*N*-carboxyanhydride (BLG-NCA) was synthesized according to the literature.[41,42] All other chemicals were obtained from

https://doi.org/10.1021/jacs.1c06020
J. Am. Chem. Soc. 2021, 143, 14684−14693

Adamas-beta and purified according to conventional methods or used as received.

Polymer Synthesis. The PBLG-*b*-PEG copolymers ($PBLG_{301}$-*b*-PEG_{113}, M_n = 71 kDa, $Đ$ = 1.25, $PBLG_{164}$-*b*-PEG_{113}, M_n = 41 kDa, $Đ$ = 1.19, and $PBLG_{320}$-*b*-PEG_{226}, M_n = 80 kDa, $Đ$ = 1.26) were synthesized using ring-opening polymerization of BLG-NCA initiated by anhydrous mPEG-NH_2 macroinitiator in anhydrous 1,4-dioxane solution. The reaction was carried out under a dry nitrogen atmosphere for 3 days at 15 °C. The reaction was stopped by pouring the reaction mixture into a large amount of anhydrous ethanol to precipitate the polymers out. The polymers were purified by two successive cycles of dissolution in chloroform followed by precipitation into a large volume of anhydrous methanol.

Polymer Characterization. The number-average molecular weight (M_n) of the block copolymer was evaluated using ^{1}H NMR measurement (Avance 500, Bruker) in $CDCl_3$ (Figure S16). Since the M_n of PEG block was known, the M_n of PBLG block could be calculated by the peak intensity ratio of the methylene proton signal (5.1 ppm) of PBLG to that of the ethylene proton signal (3.6 ppm) of PEG.[43] By varying the ratio of NCA/macroinitiator, a series of PBLG-*b*-PEG block copolymers were obtained (Table S1). The molecular weight distributions ($Đ$) of the polypeptide block copolymers were measured by gel permeation chromatography (PL-GPC, Varian, using PBLG standards synthesized in our group and characterized both by static light scattering and viscosity measurements) with DMF as eluant at a rate of 1 mL/min. All the samples show monomodal molecular weight distributions (Figure S17).

Turbidity Measurements (OD). To determine the critical water content (CWC) for the aggregation of block copolymers, turbidity measurements were performed. PBLG-*b*-PEG copolymers were first dissolved in a mixed solvent of THF/DMF = 7/3 (v/v) at a concentration of 0.05 mg mL^{-1}. Then 2 mL of polymer solution was added to a quartz cell (path length: 1 cm). Afterward, water was added dropwise (0.01 mL per drop) with vigorous stirring. After each drop of water was added, the solution was stirred for 30 s and then left to equilibrate for 1 min or more until the optical density was stable. The optical density (turbidity) was measured with a UV−vis spectrophotometer (UV-2550 Shimadzu) at a wavelength of 300 nm.

Dynamic Light-Scattering Measurement (DLS). DLS measurements (Figure S3) were carried out on a commercial LLS spectrometer (ALV/CGS-5022) equipped with an ALV-High QE APD detector and an ALV-5000 digital correlator using a He−Ne laser (the wavelength λ = 632.8 nm) as the light source at a scattering angle of 90°.

Substrate Preparation. The PS-coated silicon substrates were prepared according to the literature by adsorbing a PS nanolayer irreversibly on a Si substrate (this PS nanolayer is insoluble in THF/DMF).[44,45] The PS films were prepared by spin-coating the polymer solution onto Si substrates, which were cleaned by immersion in a hot piranha solution (i.e., H_2SO_4/H_2O_2 = 3/1 v/v) for 30 min, rinsed with a great amount of deionized water, and dried with a nitrogen gun. The spin-cast PS films were then heat-treated at ∼160 °C for 3 days under vacuum. Afterward, the films were soaked in a large volume of toluene and rinsed more than 10 times. The obtained PS-coated silicon substrates were dried in a vacuum oven at 50 °C for 24 h to remove any excess solvent before further experiments. The PS nanolayer possessed an ultrasmooth surface (roughness < 1 nm) with a thickness of ∼16 nm (Figure S18). The PS nanolayer was insoluble (stable) in THF and DMF. The same approach was used to prepare the PMMA and P2VP nanolayers (Figure S19).

Self-Assembly Experiments. In a typical self-assembly procedure, PBLG-*b*-PEG was first dissolved in a 7/3 (v/v) mixture of THF and DMF at a concentration c = 0.05 mg mL^{-1}. Three milliliters of the polymer solution at 15 °C was then poured into a beaker containing a PS-coated silicon substrate facing upward. To avoid solvent evaporation, the beaker was sealed. Afterward, 400 μL of water was added dropwise into the copolymer solution using an injection pump at a rate of 40 μL/min. Samples were incubated for various times before characterization.

Delayed Exposure Experiment. The experiment was performed in two steps. For the first step, we first masked one-half of the PS-coated silicon substrate with a clean silicon wafer. A clip was used to keep these two substrates in close contact in a lap shear joint geometry (Figure S6). The substrates were washed 3 times with toluene and dried under vacuum. We then immersed the clipped substrates into the unimer solution and added water dropwise up to 13.3 vol %. The second step started once the water was added: we removed the masking silicon wafer and rinsed the PS-coated silicon substrate with the same solvent mixtures, i.e., THF/DMF/water. The PS-coated silicon substrate was then quickly reimmersed in the micelle solution and incubated for 2 h before imaging by AFM (Figure 2e,f). To verify that micelles were present on the exposed section of the substrate at the end of the dropwise addition of water, we performed a parallel delayed exposure experiment that we stopped after step 1 (Figure 2c,d).

Effect of Unimer Addition. A PS-coated silicon substrate covered with short seeds ($L_n \approx$ 620 nm, Figure 4a,c) was immersed in a THF/DMF/water solution (THF/DMF = 7/3 v/v, water content = 13.3 vol %). A 50 μL unimer solution of $PBLG_{301}$-*b*-PEG_{113} in THF (c = 1 mg mL^{-1}) was then injected into the solution. After 2 h of incubation time the substrate was taken out of the solution and characterized by AFM (Figure 4b,d).

Observation Techniques. AFM images were obtained with an XE-100 AFM instrument (Park Systems), employing noncontact mode. The scan rate was 0.5 Hz. The images were analyzed using a professional software (XEI, Park Systems). The morphologies of the aggregates formed in solution were characterized by transmission electron microscopy (TEM) (JEM-1400, JEOL) operated at an accelerating voltage of 100 kV. The samples were prepared by depositing a drop of the solution on a TEM grid and allowing it to dry at room temperature.

Length Analysis of the Micelles. The micelle lengths were evaluated from AFM images using the Image-Pro Plus software. For each micelle population, more than 300 objects were measured to calculate the micelle lengths. The number-averaged length, L_n, the weight-averaged length, L_w, and the length distributions, $Đ_L$, were calculated using the following equations

$$L_n = \frac{\sum_{i=1}^{n} N_i L_i}{\sum_{i=1}^{n} N_i},\quad L_w = \frac{\sum_{i=1}^{n} N_i L^2{}_i}{\sum_{i=1}^{n} N_i L_i},\quad Đ_L = \frac{L_w}{L_n}$$

where N_i is the number of micelles of length L_i and n is the number of micelles examined in each sample.

Computer Simulations. Brownian dynamics (BD) simulation is a coarse-grained mesoscopic simulation method.[22,27] In the coarse-grained model, each bead represents a cluster of atoms and is connected by a harmonic spring potential. In this work, a BD model containing six rigid beads and three coil beads (denoted as R_6C_3) was constructed to represent the $PBLG_{301}$-*b*-PEG_{113} block copolymer. We set an attractive Lennard-Jones (LJ) potential for rod−rod (R−R) interactions to simulate the hydrophobicity of the rod blocks, while the interactions between C and C blocks (C−C interactions) were modeled with a purely repulsive LJ potential, thus accounting for the solvophilic nature of the PEG coil blocks. The incompatibility between PBLG and PEG blocks was simulated by setting the R−C interaction with a purely repulsive potential. The PS-coated silicon substrate was modeled as a square plane formed by orderly packed P beads. The absorption interaction between the PBLG blocks and the PS-coated silicon substrate (R−P interactions) was modeled by setting an attractive LJ potential. The time evolution of the beads obeyed the Langevin equation which includes all the potentials, the friction constant, and the noise term. The simulations were conducted in a box with periodic boundary conditions, and the NVT ensemble was adopted. In the simulations, over 1.0×10^6 BD simulation steps ($5.0 \times 10^4\tau$, τ is the unit of time in the simulation) were carried out to ensure that the system reached the equilibrium state. Detailed simulation information can be found in the Supporting Information.

https://doi.org/10.1021/jacs.1c06020
J. Am. Chem. Soc. 2021, 143, 14684−14693

■ ASSOCIATED CONTENT

Supporting Information

The Supporting Information is available free of charge at https://pubs.acs.org/doi/10.1021/jacs.1c06020.

Additional discussion; characterization data; supporting figures and tables (PDF)

■ AUTHOR INFORMATION

Corresponding Authors

Jiaping Lin − *Shanghai Key Laboratory of Advanced Polymeric Materials, Key Laboratory for Ultrafine Materials of Ministry of Education, Frontiers Science Center for Materiobiology and Dynamic Chemistry, School of Materials Science and Engineering, East China University of Science and Technology, Shanghai 200237, China;* orcid.org/0000-0001-9633-4483; Email: jlin@ecust.edu.cn

Chunhua Cai − *Shanghai Key Laboratory of Advanced Polymeric Materials, Key Laboratory for Ultrafine Materials of Ministry of Education, Frontiers Science Center for Materiobiology and Dynamic Chemistry, School of Materials Science and Engineering, East China University of Science and Technology, Shanghai 200237, China;* orcid.org/0000-0001-9008-6327; Email: caichunhua@ecust.edu.cn

Gerald Guerin − *Shanghai Key Laboratory of Advanced Polymeric Materials, Key Laboratory for Ultrafine Materials of Ministry of Education, Frontiers Science Center for Materiobiology and Dynamic Chemistry, School of Materials Science and Engineering, East China University of Science and Technology, Shanghai 200237, China;* orcid.org/0000-0003-4997-0561; Email: gguerin@ecust.edu.cn

Authors

Zhengmin Tang − *Shanghai Key Laboratory of Advanced Polymeric Materials, Key Laboratory for Ultrafine Materials of Ministry of Education, Frontiers Science Center for Materiobiology and Dynamic Chemistry, School of Materials Science and Engineering, East China University of Science and Technology, Shanghai 200237, China*

Liang Gao − *Shanghai Key Laboratory of Advanced Polymeric Materials, Key Laboratory for Ultrafine Materials of Ministry of Education, Frontiers Science Center for Materiobiology and Dynamic Chemistry, School of Materials Science and Engineering, East China University of Science and Technology, Shanghai 200237, China;* orcid.org/0000-0001-6852-8301

Yuan Yao − *Shanghai Key Laboratory of Advanced Polymeric Materials, Key Laboratory for Ultrafine Materials of Ministry of Education, Frontiers Science Center for Materiobiology and Dynamic Chemistry, School of Materials Science and Engineering, East China University of Science and Technology, Shanghai 200237, China;* orcid.org/0000-0001-9959-4707

Xiaohui Tian − *Shanghai Key Laboratory of Advanced Polymeric Materials, Key Laboratory for Ultrafine Materials of Ministry of Education, Frontiers Science Center for Materiobiology and Dynamic Chemistry, School of Materials Science and Engineering, East China University of Science and Technology, Shanghai 200237, China*

Shaoliang Lin − *Shanghai Key Laboratory of Advanced Polymeric Materials, Key Laboratory for Ultrafine Materials of Ministry of Education, Frontiers Science Center for Materiobiology and Dynamic Chemistry, School of Materials Science and Engineering, East China University of Science and Technology, Shanghai 200237, China;* orcid.org/0000-0003-3374-9934

Complete contact information is available at: https://pubs.acs.org/10.1021/jacs.1c06020

Author Contributions

†Z.T. and L.G. contributed equally to this work.

Notes

The authors declare no competing financial interest.

■ ACKNOWLEDGMENTS

This work was supported by the National Natural Science Foundation of China (51621002, 51833003, 52073095, and 21975073). Support from "the Fundamental Research Funds for the Central Universities" (50321041918013) and projects of Shanghai municipality (20YF1410700, 20ZR1471300) are also appreciated. The authors thank Professor Mitchell A. Winnik and Dr. Shaofei Song for their valuable comments and suggestions.

■ REFERENCES

(1) Discher, D. E.; Janmey, P.; Wang, Y. Tissue Cells Feel and Respond to the Stiffness of Their Substrate. *Science* **2005**, *310* (5751), 1139−1143.

(2) Brunetti, V.; Maiorano, G.; Rizzello, L.; Sorce, B.; Sabella, S.; Cingolani, R.; Pompa, P. P. Neurons Sense Nanoscale Roughness with Nanometer Sensitivity. *Proc. Natl. Acad. Sci. U. S. A.* **2010**, *107* (14), 6264−6269.

(3) Zygourakis, K.; Bizios, R.; Markenscoff, P. Proliferation of Anchorage-Dependent Contact-Inhibited Cells: I. Development of Theoretical Models Based on Cellular Automata. *Biotechnol. Bioeng.* **1991**, *38* (5), 459−470.

(4) Discher, D. E.; Eisenberg, A. Polymer Vesicles. *Science* **2002**, *297* (5583), 967−973.

(5) Zhang, L.; Eisenberg, A. Multiple Morphologies of "Crew-Cut" Aggregates of Polystyrene-b-Poly(Acrylic Acid) Block Copolymers. *Science* **1995**, *268* (5218), 1728−1731.

(6) Guerin, G.; Wang, H.; Manners, I.; Winnik, M. A. Fragmentation of Fiberlike Structures: Sonication Studies of Cylindrical Block Copolymer Micelles and Behavioral Comparisons to Biological Fibrils. *J. Am. Chem. Soc.* **2008**, *130* (44), 14763−14771.

(7) Tan, P.; Hong, L. Modeling Fibril Fragmentation in Real-Time. *J. Chem. Phys.* **2013**, *139* (8), 084904.

(8) Cai, J.; Li, C.; Kong, N.; Lu, Y.; Lin, G.; Wang, X.; Yao, Y.; Manners, I.; Qiu, H. Tailored Multifunctional Micellar Brushes via Crystallization-Driven Growth from a Surface. *Science* **2019**, *366* (6469), 1095−1098.

(9) Jia, L.; Zhao, G.; Shi, W.; Coombs, N.; Gourevich, I.; Walker, G. C.; Guerin, G.; Manners, I.; Winnik, M. A. A Design Strategy for the Hierarchical Fabrication of Colloidal Hybrid Mesostructures. *Nat. Commun.* **2014**, *5* (1), 3882.

(10) El-Zubir, O.; Kynaston, E. L.; Gwyther, J.; Nazemi, A.; Gould, O. E. C.; Whittell, G. R.; Horrocks, B. R.; Manners, I.; Houlton, A. Bottom-up Device Fabrication via the Seeded Growth of Polymer-Based Nanowires. *Chem. Sci.* **2020**, *11* (24), 6222−6228.

(11) Luk, Y.-Y.; Abbott, N. L. Surface-Driven Switching of Liquid Crystals Using Redox-Active Groups on Electrodes. *Science* **2003**, *301* (5633), 623−626.

(12) Bryan-Brown, G. P.; Wood, E. L.; Sage, I. C. Weak Surface Anchoring of Liquid Crystals. *Nature* **1999**, *399* (6734), 338−340.

(13) Son, J.-H.; Zin, W.-C.; Takezoe, H.; Song, J.-K. Alignment of Liquid Crystals Using a Molecular Layer with Patterned Molecular Density. *Adv. Mater.* **2012**, *24* (45), 6105−6110.

(14) Tang, Z.; Xu, Z.; Cai, C.; Lin, J.; Yao, Y.; Yang, C.; Tian, X. 2D Chiral Stripe Nanopatterns Self-Assembled from Rod-Coil Block

Copolymers on Microstripes. *Macromol. Rapid Commun.* **2020**, *41* (19), 2000349.
(15) Wang, L.; Tang, Z.; Li, D.; Lin, J.; Guan, Z. Adsorption and Ordering of Amphiphilic Rod−Coil Block Copolymers on a Substrate: Conditions for Well-Aligned Stripe Nanopatterns. *Nanoscale* **2020**, *12* (24), 13119−13128.
(16) *Fundamentals of Controlled/Living Radical Polymerization*; RSC Polymer Chemistry Series; The Royal Society of Chemistry: Cambridge, 2013. DOI: 10.1039/9781849737425.
(17) Gadt, T.; Ieong, N.; Cambridge, G.; Winnik, M.; Manners, I. Complex and Hierarchical Micelle Architectures from Diblock Copolymers Using Living, Crystallization-Driven Polymerizations. *Nat. Mater.* **2009**, *8* (2), 144−150.
(18) Arno, M. C.; Inam, M.; Coe, Z.; Cambridge, G.; Macdougall, L. J.; Keogh, R.; Dove, A. P.; O'Reilly, R. K. Precision Epitaxy for Aqueous 1D and 2D Poly(ϵ-Caprolactone) Assemblies. *J. Am. Chem. Soc.* **2017**, *139* (46), 16980−16985.
(19) He, W.-N.; Xu, J.-T. Crystallization Assisted Self-Assembly of Semicrystalline Block Copolymers. *Prog. Polym. Sci.* **2012**, *37* (10), 1350−1400.
(20) Cai, C.; Li, Y.; Lin, J.; Wang, L.; Lin, S.; Wang, X.-S.; Jiang, T. Simulation-Assisted Self-Assembly of Multicomponent Polymers into Hierarchical Assemblies with Varied Morphologies. *Angew. Chem., Int. Ed.* **2013**, *52* (30), 7732−7736.
(21) Lin, S.; Numasawa, N.; Nose, T.; Lin, J. Brownian Molecular Dynamics Simulation on Self-Assembly Behavior of Rod-coil Diblock Copolymers. *Macromolecules* **2007**, *40* (5), 1684−1692.
(22) Ding, W.; Lin, S.; Lin, J.; Zhang, L. Effect of Chain Conformational Change on Micelle Structures: Experimental Studies and Molecular Dynamics Simulations. *J. Phys. Chem. B* **2008**, *112* (3), 776−783.
(23) Gao, L.; Lin, J.; Zhang, L.; Wang, L. Living Supramolecular Polymerization of Rod−Coil Block Copolymers: Kinetics, Origin of Uniformity, and Its Implication. *Nano Lett.* **2019**, *19* (3), 2032−2036.
(24) Gao, L.; Gao, H.; Lin, J.; Wang, L.; Wang, X.-S.; Yang, C.; Lin, S. Growth and Termination of Cylindrical Micelles via Liquid-Crystallization-Driven Self-Assembly. *Macromolecules* **2020**, *53* (20), 8992−8999.
(25) Wang, X.; Guerin, G.; Wang, H.; Wang, Y.; Manners, I.; Winnik, M. A. Cylindrical Block Copolymer Micelles and Co-Micelles of Controlled Length and Architecture. *Science* **2007**, *317* (5838), 644−647.
(26) Gilroy, J.; Gadt, T.; Whittell, G.; Chabanne, L.; Mitchels, J.; Richardson, R.; Winnik, M.; Manners, I. Monodisperse Cylindrical Micelles by Crystallization-Driven Living Self-Assembly. *Nat. Chem.* **2010**, *2* (7), 566−570.
(27) Grest, G. S.; Lacasse, M.; Kremer, K.; Gupta, A. M. Efficient Continuum Model for Simulating Polymer Blends and Copolymers. *J. Chem. Phys.* **1996**, *105* (23), 10583−10594.
(28) Zhang, J.; Chen, X.-F.; Wei, H.-B.; Wan, X.-H. Tunable Assembly of Amphiphilic Rod−Coil Block Copolymers in Solution. *Chem. Soc. Rev.* **2013**, *42* (23), 9127−9154.
(29) Johnson, B. K.; Prud'homme, R. K. Mechanism for Rapid Self-Assembly of Block Copolymer Nanoparticles. *Phys. Rev. Lett.* **2003**, *91* (11), 118302.
(30) Riess, G. Micellization of Block Copolymers. *Prog. Polym. Sci.* **2003**, *28* (7), 1107−1170.
(31) Li, L.; Zhong, Y.; Li, J.; Chen, C.; Zhang, A.; Xu, J.; Ma, Z. Thermally Stable and Solvent Resistant Honeycomb Structured Polystyrene Films via Photochemical Cross-Linking. *J. Mater. Chem.* **2009**, *19* (39), 7222−7227.
(32) Besenius, P. Controlling Supramolecular Polymerization through Multicomponent Self-Assembly. *J. Polym. Sci., Part A: Polym. Chem.* **2017**, *55* (1), 34−78.
(33) Ganda, S.; Stenzel, M. H. Concepts, Fabrication Methods and Applications of Living Crystallization-Driven Self-Assembly of Block Copolymers. *Prog. Polym. Sci.* **2020**, *101*, 101195.
(34) Street, S. T. G.; He, Y.; Jin, X.-H.; Hodgson, L.; Verkade, P.; Manners, I. Cellular Uptake and Targeting of Low Dispersity, Dual Emissive, Segmented Block Copolymer Nanofibers. *Chem. Sci.* **2020**, *11* (32), 8394−8408.
(35) Li, Z.; Sun, L.; Zhang, Y.; Dove, A. P.; O'Reilly, R. K.; Chen, G. Shape Effect of Glyco-Nanoparticles on Macrophage Cellular Uptake and Immune Response. *ACS Macro Lett.* **2016**, *5* (9), 1059−1064.
(36) Rideau, E.; Dimova, R.; Schwille, P.; Wurm, F. R.; Landfester, K. Liposomes and Polymersomes: A Comparative Review towards Cell Mimicking. *Chem. Soc. Rev.* **2018**, *47* (23), 8572−8610.
(37) Nazemi, A.; Boott, C. E.; Lunn, D. J.; Gwyther, J.; Hayward, D. W.; Richardson, R. M.; Winnik, M. A.; Manners, I. Monodisperse Cylindrical Micelles and Block Comicelles of Controlled Length in Aqueous Media. *J. Am. Chem. Soc.* **2016**, *138* (13), 4484−4493.
(38) Shao, J.; Cao, S.; Williams, D. S.; Abdelmohsen, L. K. E. A.; van Hest, J. C. M. Photoactivated Polymersome Nanomotors: Traversing Biological Barriers. *Angew. Chem., Int. Ed.* **2020**, *59* (39), 16918−16925.
(39) Jin, X.-H.; Price, M. B.; Finnegan, J. R.; Boott, C. E.; Richter, J. M.; Rao, A.; Menke, S. M.; Friend, R. H.; Whittell, G. R.; Manners, I. Long-Range Exciton Transport in Conjugated Polymer Nanofibers Prepared by Seeded Growth. *Science* **2018**, *360* (6391), 897−900.
(40) Shaikh, H.; Jin, X.-H.; Harniman, R. L.; Richardson, R. M.; Whittell, G. R.; Manners, I. Solid-State Donor−Acceptor Coaxial Heterojunction Nanowires via Living Crystallization-Driven Self-Assembly. *J. Am. Chem. Soc.* **2020**, *142* (31), 13469−13480.
(41) Lin, J.; Abe, A.; Furuya, H.; Okamoto, S. Liquid Crystal Formation Coupled with the Coil-helix Transition in the Ternary System Poly(γ-Benzyl l-Glutamate)/Dichloroacetic Acid/Dichloroethane. *Macromolecules* **1996**, *29* (7), 2584−2589.
(42) Cai, C.; Wang, L.; Lin, J.; Zhang, X. Morphology Transformation of Hybrid Micelles Self-Assembled from Rod−Coil Block Copolymer and Nanoparticles. *Langmuir* **2012**, *28* (9), 4515−4524.
(43) Cai, C.; Zhu, W.; Chen, T.; Lin, J.; Tian, X. Synthesis and Self-Assembly Behavior of Amphiphilic Polypeptide-Based Brush-Coil Block Copolymers. *J. Polym. Sci., Part A: Polym. Chem.* **2009**, *47* (22), 5967−5978.
(44) Housmans, C.; Sferrazza, M.; Napolitano, S. Kinetics of Irreversible Chain Adsorption. *Macromolecules* **2014**, *47* (10), 3390−3393.
(45) Fujii, Y.; Yang, Z.; Leach, J.; Atarashi, H.; Tanaka, K.; Tsui, O. K. C. Affinity of Polystyrene Films to Hydrogen-Passivated Silicon and Its Relevance to the Tg of the Films. *Macromolecules* **2009**, *42* (19), 7418−7422.

https://doi.org/10.1021/jacs.1c06020
J. Am. Chem. Soc. 2021, 143, 14684−14693